Effect of Coordination Environment on the Electronic Structure and Properties of Mo_6-Based Systems: A Density Functional Treatment

L. M. Robinson, R. L. Bain, D. F. Shriver, and D. E. Ellis*

Department of Chemistry and Materials Research Center Northwestern University, Evanston, Illinois 60208

Received June 10, 1994[⊗]

A comparison of first principles density functional (DV−Xα) electronic structure calculations for six clusters of the general form $[Mo_6Cl^i_8L^a_6]^n$ ($n = 0, -1, -2$) is presented. Substitution of different neutral and anionic axial ligands (L^a), such as Cl^-, Br^-, I^-, PR_3, and 4,4′-bipyridine, significantly affects calculated electronic structure and experimentally determined optical transitions of the clusters. In the extreme case, the model of two cluster units bridged by a 4,4′-bipyridine ligand predicts a band-type structure with facile charge transport between metal cores. DV−Xα results also predict a closed-shell ground state configuration and a dipole-forbidden LUMO to HOMO transition for the $[Mo_6Cl^i_8Y^a_6]^{2-}$ (Y = Cl, Br, I) clusters, which is thought to cause the unusually long-lived excited states of these species. Effects of electronic relaxation, spin−spin, and spin−orbit coupling on the symmetry and energy of the excited state are discussed. Trends in HOMO/LUMO characteristics, net atomic charges, Mulliken populations, and density of states distributions are examined. General trends in predicted absorption energies are corroborated by experimental values, but more precise values will require study of excited state geometry.

Introduction

The molybdenum halide clusters $[Mo_6X^i_8Y^a_6]^{2-}$, in which inner halide (i) ligands cap the eight triangular faces of an octahedral array of metal atoms, and the outer (a) ligands cap the vertices of the Mo_6 octahedron, have been the subject of diverse research efforts (Figure 1). Interest in this system and other discrete metal clusters derives, in part, from their present and potential use as molecular building blocks in extended networks. Depending upon the nature of the building blocks, the multicluster systems exhibit interesting physical properties. As an example, the Chevrel phases, such as $PbMo_6S_8$, are superconductors at relatively high temperatures and coercive fields.[1] These compounds are extended solids in which the face-capping sulfur atoms from one cluster serve as outer ligands of adjacent clusters. Both the discrete $[Mo_6X^i_8Y^a_6]^{2-}$ clusters and Chevrel phases contain the $[Mo_6X_8]$ core. Understanding the electronic structure of the $[Mo_6X_8]$ subunits, which are more easily modeled theoretically and characterized experimentally, can provide insight about the properties of extended structures, and aid in efforts to synthesize new materials. The effects of outer, or axial, ligands will be critical in controlling linkages of the core structure to form extended systems; these effects are of primary interest in the present work.

Particular interest in the $[Mo_6X^i_8Y^a_6]^{2-}$ complexes is due to their long-lived electronic excited states, which give rise to interesting photoredox chemistry.[2] Upon absorption of near-UV or visible light, the $[Mo_6Cl^i_8Cl^a_6]^{2-}$ cluster exhibits an emissive lifetime of 180 μs, one of the longest lifetimes known for any transition metal complex.[2b] Diverse research efforts, both experimental and theoretical in nature, have been devoted to elucidating the nature of this emissive excited state. Spectroscopy,[2] molecular orbital calculations,[3] and energy transfer experiments[4] indicate that emission occurs via decay of a spin triplet state. Initial energy absorption is thought to involve ligand-to-metal charge transfer (LMCT).[4] It has been observed that the absorption maximum shifts as X^i and/or X^a ligands are varied, while emission energies are relatively insensitive to changes in halide ligands.[2] Emissive energy is thought to correspond roughly to the gap between the HOMO and LUMO states; however, multiplet energies are needed for quantitative comparisons between theory and experiment.

Recent synthetic advances have broadened the range of ligands that can be introduced into the axial positions and thus present the possibility of altering the photophysical properties of the cluster. Specifically, Johnston *et al.* reported the synthesis of a substitutionally labile hexanuclear molybdenum cluster $[Mo_6Cl^i_8(OSO_2CF_3)^a_6]^{2-}$.[5] The triflate ligands in these clusters are readily displaced by a variety of anionic ligands, including halides, pseudohalides, alkoxides, and carboxylates. The triflate ligands can also be displaced by neutral ligands such as phosphines, phosphine oxides, and amine oxides. Interestingly, exchange of the axial triflates with the complex ligand $[NCMn(\eta^5\text{-cp})(CO)_2]^-$ shifts the absorption maximum of the cluster approximately 100 nm, from the near-UV into the visible region.[6] The new triflate precursor not only provides the opportunity to "tune" the photophysical properties of the cluster by varying axial ligands, but also lends itself to the synthesis

[⊗] Abstract published in *Advance ACS Abstracts,* September 1, 1995.

(1) (a) Chevrel, R.; Hirrien, M.; Sergent, M. *Polyhedron* **1986**, *5*, 87−94. (b) Hughbanks, T.; Hoffmann, R. J. *J. Am. Chem. Soc.* **1983**, *105*, 1150.

(2) (a) Maverick, A. W.; Najdzionek, J. S.; MacKenzie, D.; Nocera, D. G.; Gray, H. B. *J. Am. Chem. Soc.* **1983**, *105*, 1878−1882. (b) Maverick, A. W.; Gray, H. B. *J. Am. Chem. Soc.* **1981**, *103*, 1298−1300. (c) Nocera, D. G.; Gray, H. B. *J. Am. Chem. Soc.* **1984**, *106*, 824−825. (d) Zietlow, T. C.; Nocera, D. G.; Gray, H. B. *Inorg. Chem.* **1986**, *25*, 1351−1354. (e) Zietlow, T. C.; Hopkins, M. D.; Gray, H. B. *J. Solid State Chem.* **1985**, *57*, 112. (f) Mussell, R. D., Nocera, D. C. *J. Am. Chem. Soc.* **1988**, *110*, 2764−2772. (g) Jackson, J. A.; Turro, C.; Newsham, M. D.; Nocera, D. G. *J. Phys. Chem.* **1990**, *94*, 2500−2507. (h) Mussell, R. D.; Nocera, D. G. *Inorg. Chem.* **1990**, *29*, 3711−3717.

(3) (a) Azumi, T.; Saito, Y. *J. Phys. Chem.* **1988**, *103*, 1298−1300. (b) Saito, Y.; Tanaka, H. K.; Sasaki, Y.; Azumi, T. *J. Phys. Chem.* **1985**, *89*, 4413−4415.

(4) (a) Zietlow, T. C.; Hopkins, M. D.; Gray, H. B. *J. Solid State Chem.* **1985**, *57*, 112−119. (b) References 2g and 2h.

(5) Johnston, D. H.; Gaswick, D. C.; Lonergan, M.; Stern, C. L.; Shriver, D. F. *Inorg. Chem.* **1992**, *31*, 1869.

(6) Johnston, D. H.; Stern, C. L.; Shriver, D. F. *Inorg. Chem.* **1993**, *32*, 5170−5175.

0020-1669/95/1334-5588$09.00/0

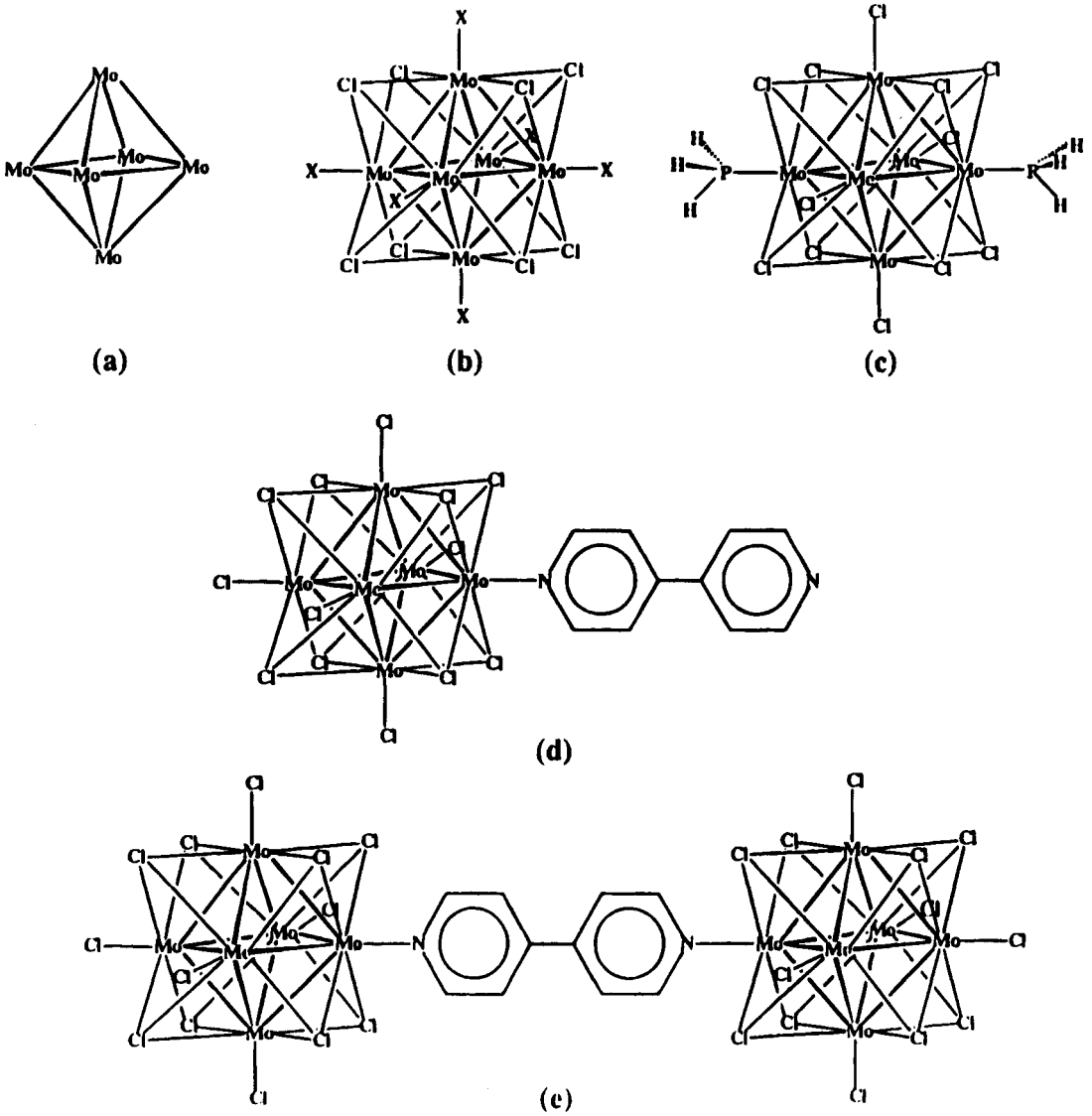

Figure 1. Representations of (a) bare Mo_6 cluster, (b) $[Mo_6Cl_8X_6]^{2-}$ (X = Cl, Br, I), (c) $[Mo_6Cl_8Cl_4(PH_3)_2]$, (d) $[Mo_6Cl_8Cl_5(C_{10}H_8N_2)]^-$, and (e) $\{[Mo_6Cl_8Cl_5]_2(C_{10}H_8N_2)\}^{2-}$.

of two- and three-dimensional arrays through the use of bridging ligands. While such bridged structures are unlikely to be superconductors, as in the case of the Chevrel phases, they should display interesting photophysical behavior.

This synthetic effort involving the triflate cluster can both aid and be aided by the development of a reliable electronic structure model. Spectroscopic and other experimental data for the range of axially substituted clusters now accessible is essential to "calibrating" and fine-tuning a theoretical model. Once the model is refined, however, theory can help guide synthetic efforts by predicting the effects of various ligands on optical transitions. Such a model requires more precise calculation of the cluster's electronic structure than has previously been undertaken.

A variety of electronic structure calculations, including the Cotton-Haas, Fenske–Hall, SCF–Xα–SW and extended Hückel approximations, have been performed on the $[Mo_6X^i_8Y^a_6]^{2-}$ system.[7] Predicted symmetries and metal/ligand character of the HOMO and LUMO, as well as the HOMO/LUMO energy gap, vary considerably among these calculations. Because the electronic structure of these cluster compounds is characterized by a substantial number of molecular orbitals in the vicinity of the HOMO and LUMO, slight variations in the applied approximation can yield significantly different results. While electronic structure calculations containing small errors may still yield a good qualitative picture of the electronic structure, they may fail to predict the correct symmetry of the HOMO or LUMO or quantitatively reproduce spectroscopic data.

Fortunately, recent advances in density functional methodology make more precise calculations possible. As we have reported previously,[8,9] the discrete variational (DV–Xα) method coupled with first principles local density (LD) theory is well-suited to ionic species and covalently bonded systems such as the Mo_6 system. For example, recent studies on octahedral gold cluster compounds have shown the (previously unsuspected)

(7) (a) Cotton, F. A.; Stanley, G. S. *Chem. Phys. Lett.* **1978**, *3*, 450–453. (b) Siefert, G.; Grossmann, G. *J. Mol. Struct.* **1980**, *64*, 93–102. (c) Cotton, F. A.; Haas, T. E. *Inorg. Chem.* **1964**, *3*, 10–17. (d) Guggenberger, L. J.; Sleight, A. W. *Inorg. Chem.* **1969**, *10*, 2041–2044. (e) Bursten, B. E.; Cotton, F. A.; Stanley, G. G. *Isr. J. Chem.* **1980**, *19*, 132–142. (f) Reference 1b. (g) Hall, M. B.; Fenske, R. F. *Inorg. Chem.* **1972**, *11*, 768.

(8) Gorling, A.; Rösch, N.; Ellis, D. *Inorg. Chem.* **1991**, *30*, 3986.

(9) (a) Ellis, D. E.; Cheng, H. P.; Holland, G. F. In *Physics and Chemistry of Small Clusters*; Jena, P., Rao, B. K., and Khanna, S. N., Eds.; Plenum: New York, 1987; pp 881–890. (b) Ellis, D. E.; Holland, G. F. *Chem. Scripta* **1986**, *26*, 441. (c) Holland, G. F.; Ellis, D. E.; Trogler, W. C. *J. Am. Chem. Soc.* **1986**, *108*, 1884. (d) Salahub, D. R.; Raatz, F. *Int. J. Quantum Chem. Symp.* **1984**, *18*, 173. (e) Rösch, N.; Ackermann, L.; Paachioni, G.; Dunlap, B. I. *J. Chem. Phys.* **1991**, *95*, 7004.

importance of opening the Au 5d shell to form s−d hybrid bonds with internal and external ligands in complexes such as $\{[(H_3P)Au]_6X\}^{m+}$ (X = B, C, N; m = 1, 2, 3).[8] In addition, LD models of transition metal carbonyl compounds have helped to elucidate metal−ligand interactions and local effects on magnetic moments.[9]

In the present study, we combine theory and experiment to further investigate the interesting but rather poorly defined electronic structure of the $[Mo_6Cl^i_8L^a_6]^n$ system (n = −2, −1, 0). We report our findings on the effects of ligand substitution on the metal core and metal−ligand bonding of the clusters. A series of six clusters are examined for trends in HOMO/LUMO characteristics, net atomic charge, Mulliken populations, and density of states. Predicted and experimental values of absorption and emission energies are also compared.

Experimental Section

Syntheses. $(Bu_4N)_2[Mo_6Cl^i_8Cl^a_6]$ was prepared by literature methods.[5,10] $(Bu_4N)_2[Mo_6Cl^i_8Br^a_6]$ and $(Bu_4N)_2[Mo_6Cl^i_8I^a_6]$ were synthesized according to the method of Johnston *et al.* from the "triflate" cluster precursor, $[Mo_6Cl^i_8(OSO_2CF_3)^a_6]^{2-}$.[5] $[Mo_6Cl^i_8Cl^a_4\{P(C_4H_9)_3\}^a_2]$ was prepared by the method of Saito *et al.*[11] The product consists predominantly of the trans isomer.[11]

Instrumentation. Emission spectra were recorded on a SPEX Fluoromax spectrofluorimeter with an excitation wavelength of 420 nm. Dichloromethane solutions of the compounds were placed in 1.0 cm path length quartz cells. Dichloromethane solution UV−vis spectra were obtained with a Varian Cary 1E spectrophotometer, with use of 1.0 cm matched quartz cells.

Computational Details

DV−Xα Method. This study employs an implementation of local density theory to self-consistently determine the electronic structure of molecular clusters. The first principles LD theory has proven to be a quantitative tool for describing electronic structure of atoms, molecules and solids.[12] In the discrete variational (DV−Xα) approach applied in the present calculations, the potential and wave function are expanded in variational form, without shape approximations.[13] The DV−Xα scheme derives molecular orbitals (MO) from numerically generated orbital basis sets via a linear combination of atomic orbitals (LCAO) expansion.[14] The familiar secular equation $|\mathbf{H} - \mathbf{ES}| = 0$ is solved by standard procedures.

The molecular charge density is obtained from the eigenfunctions ψ_i as

$$\varrho(r) = \sum_i f_i |\psi_i(r)|^2 \qquad (1)$$

where f_i are Fermi−Dirac occupation numbers. In order to solve the Poisson equation for the Coulomb potential efficiently, ϱ is fitted to a multicenter multipolar expansion basis. The simplest, so-called self-consistent-charge (SCC) scheme is based upon Mulliken population analysis of orbital densities, which gives a familiar and intuitive picture of effective atomic configurations.

Table 1. Optimized Numerical Atomic Orbital Basis Sets Used in SCF Cluster Calculations[a]

atom	basis set	atom	basis set
H	1s	Cl	3s 3p 3d
C	2s 2p	Br	4s 4p 4d
N	2s 2p	I	5s 5p 5d
P	3s 3p 3d	Mo	4d 5s 5p

[a] Omitted levels are treated as a frozen core, determined in the SCF effective ionic configuration.

The extension of the fit by least squares self-consistent-multipolar (SCM) methods can be carried to any desired level of precision.[15] Most of the work reported here was done in the SCC scheme; however, the diffuse π-electron structure of the bipyridine complexes required use of the extended SCM scheme.

There exist a variety of density functional approximations to the many-body exchange and correlation potential.[16] We have chosen to use the von Barth−Hedin form, which includes exchange and a simple fit to numerically determined electron−gas correlation.[17] Approximations involving more elaborate correlation terms and nonlocal (gradient) corrections were deemed unnecessary for the present exploratory studies.

The quality of the results is a function of the completeness of the bases and the numerical integration precision. Spectroscopic information, densities of states and charge and spin densities were extracted from self-consistent wave functions, using optimized extended bases (see Table 1). Integration meshes of approximately 12 000 points were used to ensure precision of better than 0.1 eV in single particle energies. In order to simplify the molecular orbital calculations of $[Mo_6Cl^i_8Cl^a_4\{P(C_4H_9)_3\}^a_2]$, the tributylphosphine groups have been replaced with PH_3 groups. This substitution should not significantly affect the values calculated.

Extended Hückel Method. Literature reports of extended Hückel calculations on related systems are limited to $[Mo_6S_8]^{4-}$,[1a] and $[Mo_6Br_{12}(H_2O)_2]^{7d}$ clusters. Because each study employed different orbital exponents and coefficient values, for purposes of comparison and consistency, we also conducted extended Hückel calculations for the $[Mo_6Cl^i_8Cl^a_6]^{2-}$, $[Mo_6Cl^i_8Br^a_6]^{2-}$, and $[Mo_6Cl^i_8I^a_6]^{2-}$ systems with a program developed by Mealli *et al.*[18]

Results and Discussion

Six cluster species were selected for this study to provide a range of different ligands and substitution patterns (see Figure 1). The "bare" metal cluster, Mo_6, provides a simple metal−metal bonding reference with which to compare the ligated complexes. The $[Mo_6Cl^i_8Y^a_6]^{2-}$ (Y = Cl, Br, I) and the neutral $[Mo_6Cl^i_8Cl^a_4(PH_3)^a_2]$ complexes are used to compare how some commonly used ligands affect the electronic structure of the cluster. Because the chloride-, bromide-, iodide-, and phosphine-substituted compounds have all been isolated and rigorously characterized experimentally, they can be used to "calibrate" theoretical predictions of physical properties. The "bipy monomer" (Figure 1d), in which one of the axial chlorides is replaced by a single, monocoordinated 4,4′-bipyridine ligand, and the "bipy dimer" (Figure 1e), a bridged structure of two clusters linked by a single 4,4′-bipyridine ligand, were examined

(10) Dorman, W. C.; McCarley, R. E. *Inorg. Chem.* **1974**, *13*, 41.
(11) Saito, T.; Nishida, M.; Yamagata, T.; Yamagata, Y. *Inorg Chem.* **1986**, *25*, 1111.
(12) (a) Painter, G. S.; Ellis, D. E. *Phys. Rev. B* **1970**, *1*, 4747. (b) Ellis, D. E. In *Electronic and Magnetic Distributions in Molecules and Crystals: Application of Diffraction Methods*; Becker, P., Ed., Plenum: New York, 1980; p 107. (c) Ellis, D. E. In *Handbook on the Physics and Chemistry of the Actinides*; Freeman, A. J., Lander, G. H., Eds.; North-Holland: Amsterdam, 1985; p 1. (d) Ellis, D. E.; Guo, J; Low, J. J. *Quantum Chemistry Approaches to Chemisorption and Heterogeneous Catalysis*; Ruette, F., Ed.; Kluwer: Dordrecht, The Netherlands, 1992; p 69.
(13) Baerends, E. J.; Ellis, D. E.; Ros, P. *Chem. Phys.* **1973**, *2*, 4.
(14) Rose'n, A; Ellis, D. E.; Adachi, H; Averill, F. W. *J. Chem. Phys.* **1976**, *65*, 3629.
(15) Delley, B; Ellis, D. E. *J. Chem. Phys.* **1982**, *76*, 1949.
(16) Parr, R. G.; Yang, W-T. *Density-Functional Theory of Atoms and Molecules*; Oxford Press: Oxford, U.K., 1989.
(17) (a) von Barth, U.; Hedin, L. *J. Phys.* **1972**, *C5*, 1629. (b) Vosko, S. J.; Wilk, L.; Nussair, M. *Can. J. Phys.* **1980**, *68*, 1200. (c) Langreth, D. C.; Mehl, M. J. *Phys. Rev. Lett.* **1981**, *47*, 446; *Phys. Rev.* **1983**, *B28*, 1809; *Phys. Rev.* **1984**, *B29*, 2310.
(18) Mealli, C.; Proserpio, D. M. *J. Chem. Educ.* **1990**, *67*, 399.

Table 2. Comparison of Net Average Atomic Charges on Cluster Atoms[a]

cluster type		net charge				
		Mo	X^i	X^a	PH_3	bipy
bare Mo_6	SCC	0				
$[Mo_6Cl^i_8Cl^a_6]^{2-}$	SCC	0.61	−0.36	−0.47		
	SCM	0.95	−0.49	−0.63		
$[Mo_6Cl^i_8Br^a_6]^{2-}$	SCC	0.55	−0.37	−0.39		
$[Mo_6Cl^i_8I^a_6]^{2-}$	SCC	0.56	−0.39	−0.37		
$[Mo_6Cl^i_8Cl^a_4(PH_3)^a_2]^{2-}$	SCC	0.62	−0.33	−0.33	1.60	
$[Mo_6Cl^i_8Cl^a_5(bipy)^a]^{1-}$	SCM	0.98[b]	−0.48	−0.49		−1.42
		0.75[c]				
		1.05[d]				
$\{[Mo_6Cl^i_8Cl^a_5]_2[(bipy)^a]\}^{2-}$	SCM	0.90[b]	−0.47	−0.50		−0.53
		0.92[c]				
		1.00[d]				

[a] Potential approximation scheme used is indicated as SCC or SCM, as described in text. [b] Mo atom bound to chloride ligand. [c] Mo atom bound to nitrogen of 4,4′-bipyridine ring. [d] Mo atom *trans* to "A".

Table 3. Comparison of Average Mulliken Populations for the Main Valence Orbitals of the Mo Atoms in Different Clusters[a]

cluster type		Mo 4d	Mo 5s	Mo 5p
bare Mo_6	SCC	5.02	0.48	0.49
$[Mo_6Cl^i_8Cl^a_6]^{2-}$	SCC	4.89	0.15	0.34
	SCM	4.73	0.11	0.21
$[Mo_6Cl^i_8Br^a_6]^{2-}$	SCC	4.92	0.18	0.35
$[Mo_6Cl^i_8I^a_6]^{2-}$	SCC	4.94	0.18	0.32
$[Mo_6Cl^i_8Cl^a_4(PH_3)^a_2]$	SCC	4.91	0.18	0.35
$[Mo_6Cl^i_8Cl^a_5(bipy)^a]^{1-}$	SCM	4.79	0.01	0.35
$\{[Mo_6Cl^i_8Cl^a_5]_2(bipy)^a\}^{2-}$	SCM	4.84	0.01	0.27

[a] Potential approximation scheme used is indicated as SCC or SCM.

to determine the degree of electronic coupling between metal clusters through the conjugated ligand bridge. The syntheses of the bipyridine derivatives are currently under investigation.

Net Atomic Charge and Mulliken Populations. In analyzing the effects of ligand substitution on the metal−metal and metal−ligand bonding of the clusters, it is useful to first look at trends in the net charges of individual atoms and the Mulliken populations of the clusters. These results are presented in Tables 2 and 3. It is important to note that the atomic charges of the chloride, bromide, iodide, and bis(phosphine) clusters were calculated using the self-consistent charge (SCC) approximation to the potential, while the bipyridine systems required use of the least squares (SCM) scheme. Preliminary SCC calculations on bipy monomer and dimer clusters showed significant displacement (in energy) of π-electron densities relative to the σ-electrons, as found in previous studies on aromatic systems.[19] SCM calculations were also made on the octahedral chloride complex, in order to verify adequacy of the simpler SCC potential for halide and phosphine complexes. We found that the SCM potential predicts slightly greater ionicity than SCC, while significant spectroscopic features are unaltered.

Although each molybdenum atom is formally in a +2 oxidation state in the ligated cluster, the LD results reveal much smaller charges, ranging from 0.55 e to 1.05 e. This is consistent with the idea that bonding in these clusters is partially covalent in nature, with significant delocalization of charge throughout the framework. Our results are also highly compatible with the DV−Xα SCC study of $[Mo_6X_8(PH_3)_6]$ (X = S and Se) complexes by Imoto *et al.*[20] Density of states analysis presented below confirms in detail the presence of extensive

(19) (a) Doris,K. A.; Delley, B.; Ratner, M. A.; Marks, T. J.; Ellis, D. E. *J. Phys. Chem.* **1984**, *88*, 3157. (b) Doris, K. A.; Ellis, D. E.; Ratner, M. A.; Marks, T. J. *J. Am. Chem. Soc.* **1984**, *106*, 2491.

(20) Imoto, H.; Saito, T.; Adachi, H. *Inorg. Chem.* **1995**, *34*, 2415.

Table 4. Percent Atomic Composition and Symmetry Type of HOMO and LUMO Orbitals

cluster type	MO	sym	Mo	X^i	X^a	PH_3
$[Mo_6Cl^i_8Cl^a_6]^{2-}$	HOMO	t_{2u}	22	10	68	
	LUMO	e_u	68	32	0	
$[Mo_6Cl^i_8Br^a_6]^{2-}$	HOMO	t_{2u}	22	11	67	
	LUMO	e_u	68	32	0	
$[Mo_6Cl^i_8I^a_6]^{2-}$	HOMO	t_{2u}	6	4	90	
	LUMO	t_{2u}	51	19	30	
$[Mo_6Cl^i_8Cl^a_4(PH_3)^a_2]$	HOMO	b_1	15	10	75	0
	LUMO	b_1	55	25	5	15

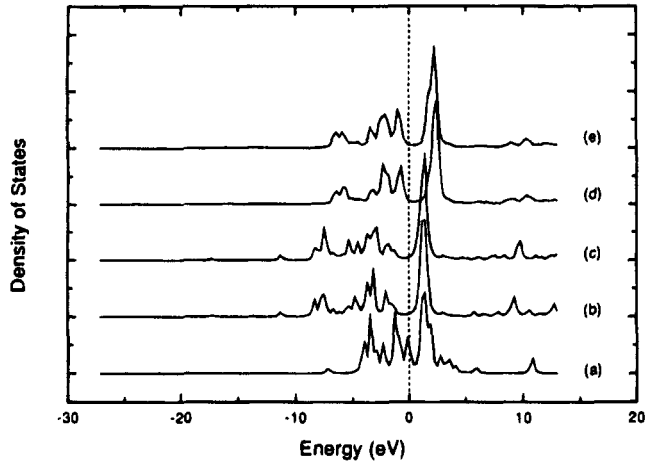

Figure 2. Density of states for Mo 4d orbitals in (a) Mo_6, (b) $[Mo_6Cl_8Cl_6]^{2-}$, (c) $[Mo_6Cl_8Cl_4(PH_3)_2]$, (d) $[Mo_6Cl_8Cl_5(C_{10}H_8N_2)]^-$, and (e) $\{[Mo_6Cl_8Cl_5]_2(C_{10}H_8N_2)\}^{2-}$.

metal-d/ligand-p covalency across the entire valence band. In general, the Mo_6 core reacts like a collective metal fragment; charge transfers driven by electron withdrawing axial ligands are rather uniformly spread over the six Mo atoms. Thus, average charges are shown in Table 2, with more detail given for the hypothetical bipy monomer and dimer. We note that ionicity of the bipy complexes is quite comparable to that of the octahedral halides, seen by comparison with SCM results for the chloride in Table 2. Comparison of the Mulliken populations of molybdenum 4d, 5s, and 5p atomic orbitals in Table 3 also reveals interesting information about the nature of bonding in the clusters. Although the d orbitals dominate the Mo valence electron density, as would be expected, the 5s and 5p contributions are also significant. These diffuse orbitals extend over the metal cluster and onto adjacent ligands, forming a "conduction electron sea" which can transport charge and energy throughout the molecular framework. With linkages formed through conjugated bridges, we expect to observe bandlike conduction mechanisms as found in many molecular metals. The pure halides display a significant "band gap"; i.e., they are insulators or large-gap semiconductors. The narrowing of the gap by ligand substitution, and formation of transport pathways by means of intercluster linkages provides ample opportunities for devising new photoactive and conductive materials.

Frontier Orbitals. The cluster frontier orbitals provide a more detailed picture of how ligands affect electronic structure. Table 4 summarizes the percent ligand and metal contribution to the HOMO and LUMO orbitals; we observe similar HOMO/LUMO characteristics for each of the clusters. The O_h halide complexes all display t_{2u} HOMO symmetry; however, many levels lie quite close in energy as seen in DOS diagrams (Figures 2−6), and internal rearrangements occur in passing from one compound to another. The HOMO's have predominantly axialligand (X^a) character, with significant metal contribution.

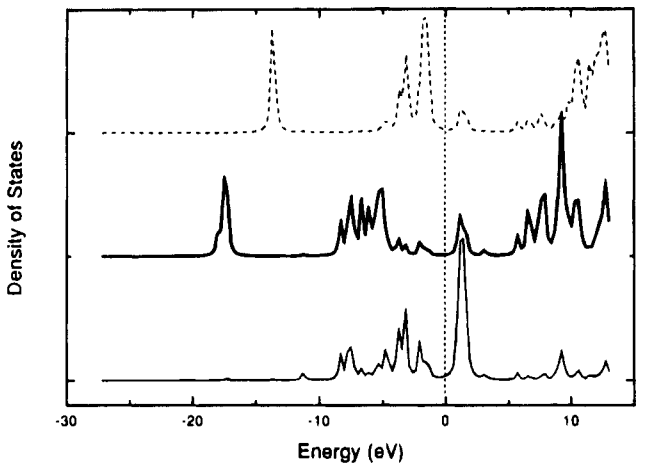

Figure 3. Partial densities of states for $[Mo_6Cl_8Cl_6]^{2-}$: Mo (light solid line), inner Cl (heavy solid line), and outer Cl (light broken line).

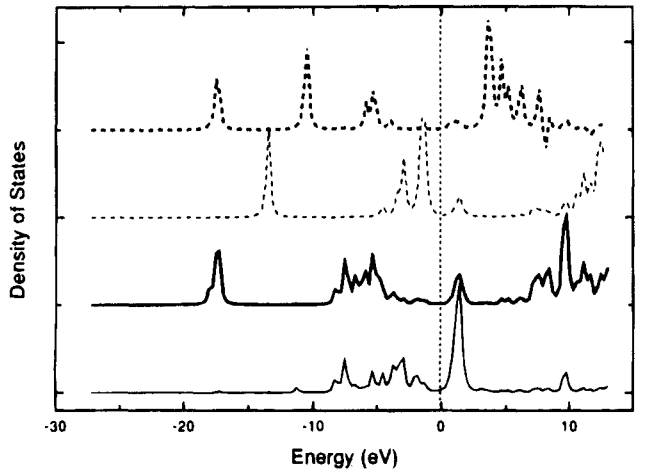

Figure 4. Partial densities of states for $[Mo_6Cl_8Cl_4(PH_3)_2]$: Mo (light solid line), inner Cl (solid heavy line), outer Cl (light broken line), and P (heavy broken line).

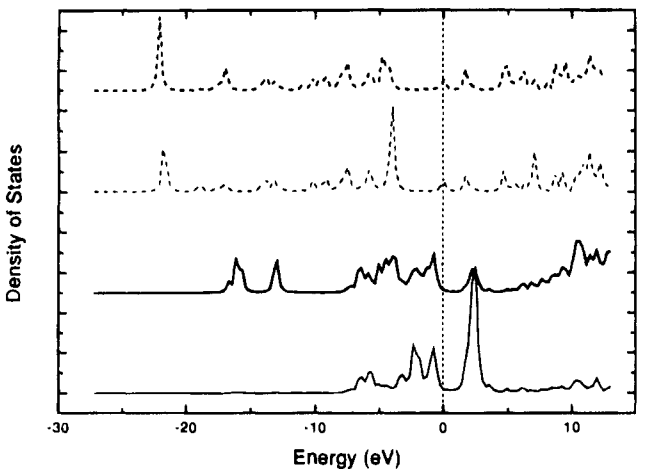

Figure 5. Partial densities of states for $[Mo_6Cl_8Cl_5(C_{10}H_8N_2)]^-$: Mo (light solid line), both inner and outer Cl (heavy solid line), coordinated N (light broken line), and uncoordinated N (heavy broken line).

In contrast, the LUMO's are primarily metal based, with significant face-bridging (X^i) character. The phosphine cluster deviates slightly, having significant contribution from the axial phosphine ligands to the LUMO. The LUMO for the chloride and bromide complexes is of e_u symmetry; however, the next excited level, of t_{1u} type, lies nearby and descends in energy with increasing ligand atomic number, becoming the LUMO for the iodide cluster.

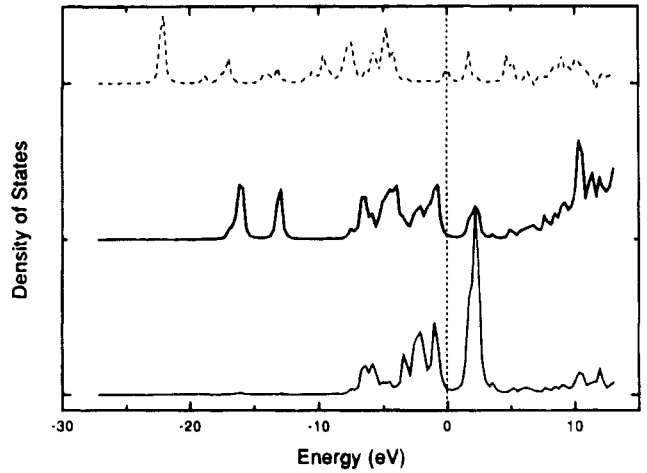

Figure 6. Partial densities of states for $\{[Mo_6Cl_8Cl_5]_2(C_{10}H_8N_2)\}^{2-}$: Mo (light solid line), both inner and outer Cl (heavy solid line), and N (light broken line).

It is interesting to compare the DV−Xα results with those obtained using other molecular orbital theories. There is general agreement regarding the magnitude of the HOMO/LUMO gap (approximately 2.0 ± 0.5 eV) and the closed shell configuration of the ground state of the $[Mo_6Cl^i_8Cl^a_6]^{2-}$ system. However, the composition of the frontier orbitals is subject to debate. The SCF−Xα−SW results are quite similar to DV−Xα, predicting a HOMO with 35% molybdenum and 65% axial ligand character.[7a] A further comparison, to the DV−Xα results of Imoto *et al.*[20] on $Mo_6S_8(PH_3)_6$, is useful. The HOMO (t_{1u}) has about 25% Mo d, 65% S sp, and 10% P sp character, while the LUMO (e_g) has 75% Mo d and 25% S sp composition. In contrast, our extended Hückel results,[21] as well as those of earlier EH calculations,[1b,7d] Cotton−Haas,[7c] and Fenske−Hall[7g] calculations predict a HOMO with predominantly metal character (approximately 80% or greater), with only small contributions from the face-bridging ligands. The predicted symmetries of the HOMO and LUMO also vary considerably among the different theoretical treatments. This comparison underscores the fact that the calculation of unambiguous electronic structures for these complex cluster systems is not straightforward.

Density of States. Although it is useful to look at the specific HOMO and LUMO orbitals as a basis for comparison between clusters, one can argue that these distinct orbitals are not adequate representations of the "frontier" states of the clusters. Because there are multiple, closely-spaced levels very near in energy to the HOMO and LUMO states, it is certain that observed electronic transition bands involve more than a single, discrete molecular orbital. For example, there are 16 occupied states (not counting degeneracy) within 5 eV of the Fermi level, and 8 empty states of significance for vis−UV transitions, and this is the *simplest* of the systems discussed here. Therefore, it is useful to look at a density of states (DOS) representation, which more clearly illustrates the overall contribution of metal and ligand states to the frontier regions above and below the HOMO/LUMO gap.

The contribution of state nl of atom ν to the DOS is represented by

$$D^{\nu}_{nl}(E) = \sum_p f^{\nu}_{nlp} L(E - \epsilon_p, \sigma) \qquad (2)$$

where $f_{nl,p}$ is the appropriate Mulliken population contribution to the pth molecular orbital. $L(E - \epsilon_p, \sigma)$ is a line shape function

(21) See extended Hückel computational details under Experimental Section.

chosen here as a Lorentzian of width $\sigma = 0.14$ eV. By summing all partial DOS, we obtain the total DOS

$$D(E) = \sum_{vnl} D^{v}_{nl} = \sum_{p} L(E - \epsilon_p, \sigma) \qquad (3)$$

A comparison of the Mo 4d DOS for different clusters with that of a "bare" metal fragment is presented in Figure 2. Several interesting features are evident. The "bare" Mo_6 cluster has a continuous 4d band typical of a metal and the Fermi energy (set to zero here) falls at a peak in the DOS. The DOS diagrams of the chloride, bromide, iodide, and bis(phosphine) clusters have very similar metal composition, with a particularly strong peak ~1.4 eV above the Fermi level, consistent with the partially occupied molybdenum d-shell, formally d^4. (For simplicity, only the chloride and phosphine clusters are shown, Figure 2, plots b and c). We can see that the metal−ligand bonding interaction has opened a gap centered on the Fermi energy, which is of course, responsible for the ~2 eV gap in the optical absorption spectra. The occupied region has broadened from ~5 eV in Mo_6 to ~9 eV in the halide complexes, indicative of strong metal−ligand interaction.

The bipyridine derivatives exhibit a slightly different 4d profile, with the d bands above and below the Fermi level shifted to higher energies. The occupied region has a width of ~7.5 eV, appreciably narrower than for the pure halides; the excited state peak broadens and moves to ~2.3 eV. The position and width of this peak is of course directly related to the energy and line width of ligand-metal charge transfer (LMCT) transitions discussed in more detail below.

Contributions typical of the pure halide complexes, from metal, face-bridging ligand (X^i), and axial ligand (X^a) shown in Figure 3 clarify the contribution of each type of atom to the electronic structure. A strong bonding mixture of X^i and Mo character is seen to form the lower half of the valence band. The X^i and X^a have relatively little DOS overlap; the greater strength of the Mo−X^i bond is indicated by the displacement of the lower (Cl 3s) valence band by ~4 eV, compared to that of X^a. The most obvious, and experimentally meaningful, result extracted from these data is the dominance of the axial ligand contribution just below the Fermi level and of the metal contribution just above the Fermi level. The DOS picture shows that numerous low-lying transitions to the excited states involve predominantly axial ligand-to-metal charge transfer (LMCT). Thus, the DV−Xα model is in agreement with the commonly accepted LMCT assignment for the intense absorption bands in the near-UV.[4] Recalling that several of the molecular orbital calculations cited previously predict a HOMO with predominantly metal character, rather than ligand character, our model appears to be an improvement upon the simpler approximations.

The bis(phosphine) cluster is analyzed in Figure 4, showing the rather mild perturbation of the Mo_6Cl_8 core and the essentially undisturbed position of the remaining Cl_4 axial ligand features. The calculations of Imoto *et al.* on $Mo_6S_8(PH_3)_6$ produce a similar phosphorus spectrum, with only small contributions to the upper valence band and intense features found deep in the valence band and several eV above E_F.

Features of the bipy monomer are analyzed in Figure 5; as mentioned earlier the Mo_6 4d structure is visibly perturbed. The occupied d-bandwidth is decreased by ~1 eV compared to pure halide and bis(phosphine) complexes, and the prominent excited state peak is broadened and shifted upward by ~1eV. Both coordinated and terminal nitrogen spectra are shown; we can see that the two components are not greatly different. From this we infer that the long range polarization and electron-withdrawing capability of bipyridine are mainly responsible for the observed core changes. Mo, Cl, and N contributions to DOS of the hypothetical bipy dimer are shown in Figure 6 and correspond nicely to those of the monomer. The distribution of bonded N 2p levels throughout the entire valence and low-lying excitation region (see Figures 5 and 6) indicate that 4,4′-bipyridine-bridged clusters should effectively couple the Mo_6 cores and provide a pathway for electron transport.

Table 5. Comparison of Predicted and Experimentally Determined Energies of Absorption[a]

cluster type	excitation energy, nm (eV) HOMO → M*	V → M*	experiment
$[Mo_6Cl^i_8Cl^a_6]^{2-}$	396 (3.13)	411 (3.02)	313 (3.96)
$[Mo_6Cl^i_8Br^a_6]^{2-}$	453 (2.74)	490 (2.53)	352 (3.55)
$[Mo_6Cl^i_8I^a_6]^{2-}$	526 (2.36)	559 (2.22)	370 (3.35)[b]
$[Mo_6Cl^i_8Cl^a_4(PH_3)^a_2]$	430 (2.88)	470 (2.64)	285 (4.35)
$[Mo_6Cl^i_8Cl^a_5(bipy)^a]^{1-}$		387 (3.20)	
$\{[Mo_6Cl^i_8Cl^a_5]_2(bipy)\}^{2-}$		387 (3.20)	

[a] DV−Xα predictions for excitation from the ground state HOMO to the first excited state DOS band maximum (M*) are given, along with the projected density of states band peak which includes all dipole-allowed transitions from states lying within the first valence band (V). [b] A higher energy peak at 280 nm obscured by solvent absorption in the spectra of the chloride and bromide substituted clusters is actually the most intense band.

Table 6. Comparison of Predicted and Experimentally Determined Emission Energies, Based on Single Particle Transition Analysis[c]

cluster type	experiment, nm (eV)	ΔE(H/L), nm (eV)	ΔE(dipole), nm (eV)
$[Mo_6Cl^i_8Cl^a_6]^{2-}$	685[a] (1.80)	513 (2.42)	470 (2.64)
	766[b] (1.61)	$t_{2u} \leftarrow e_u$	
$[Mo_6Cl^i_8Br^a_6]^{2-}$	695[a] (1.79)	532 (2.33)	484 (2.56)
	790[b] (1.57)	$t_{2u} \leftarrow e_u$	
$[Mo_6Cl^i_8I^a_6]^{2-}$	715[a] (1.74)	681 (1.82)	617 (2.01)
	823[b] (1.51)	$t_{2u} \leftarrow t_{1u}$	
$[Mo_6Cl^i_8Cl^a_4(PH_3)^a_2]$	698[a] (1.78)	663 (1.87)	663 (1.87)
		$b_1 \leftarrow b_1$	
$[Mo_6Cl^i_8Cl^a_5(bipy)^a]^{1-}$		2339 (0.53)	2339 (0.53)
		$b_1 \leftarrow a_1$	
$\{[Mo_6Cl^i_8Cl^a_5]_2(bipy)^a\}^{2-}$		2067 (0.60)	725 (1.71)
		$b_u \leftarrow a_u$	

[a] Uncorrected emission energy values obtained, this work. [b] Corrected emission energies reported in ref 21. [c] ΔE(H/L) is the LUMO ← HOMO energy, and ΔE(dipole) is the first allowed transition. See text for discussion of excited state relaxation, multiplet, and spin−orbit corrections.

Optical Transitions. We now focus on the utility of the theoretical model in predicting spectroscopic data. Experimental values for emission and absorption energies of the chloride-, bromide-, iodide-, and phosphine-substituted clusters provide a means to "calibrate" the model, so that systematic errors can be compensated. A comparison of the DV−Xα predictions (based on ground state energy levels) and experimental data is presented in Tables 5 and 6.

Energy Absorption to the Excited State. The excitation energies were first calculated according to a simple model: one-electron, dipole-allowed transitions from the HOMO to an unoccupied state. Assuming slow variation of the dipole matrix element with energy, we have defined the HOMO → M* band peak, where M* corresponds to the excited state, as the energy at which the largest density of final states occurs. Calculated values are seen to be systematically underestimated, with errors of 0.6−1.0 eV for the halides and a surprisingly large 1.5 eV for the phosphine compound. It must be noted that the "true" absorption maximum for $[Mo_6Cl^i_8I^a_6]^{2-}$ is observed at 280 nm; however, this band, with $\epsilon = 22 \times 10^4$ L mol^{-1} cm^{-1}, corresponds to a much higher energy band than the 313 nm

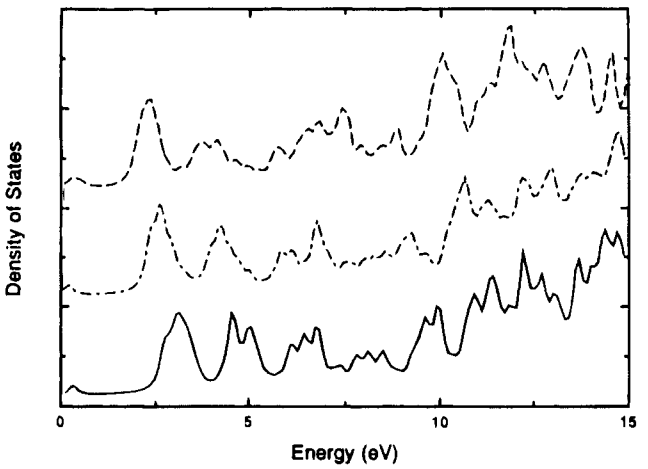

Figure 7. Dipole-allowed transitions for $[Mo_6Cl_8X_6]^{2-}$, where X = Cl (—), Br (- • -), and I (- -).

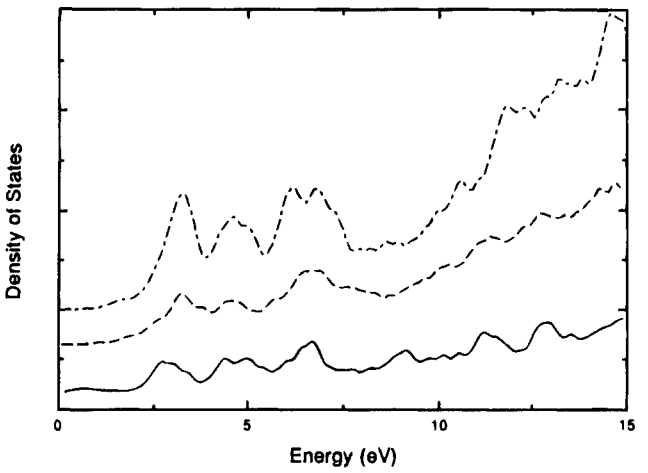

Figure 8. Dipole-allowed transitions for $[Mo_6Cl_8Cl_4(PH_3)_2]$ (—), $[Mo_6Cl_8Cl_5(C_{10}H_8N_2)]^-$ (- -), and $\{[Mo_6Cl_8Cl_5]_2(C_{10}H_8N_2)\}^{2-}$ (- • -).

and 352 nm peaks ($\epsilon = 0.32 \times 10^4$ L mol^{-1} cm^{-1}) reported for the chloride and bromide clusters, respectively.[5] The high energy band is apparently obscured by solvent absorption in the UV−vis spectra of the chloride and bromide clusters, and shifts to lower energies for the iodide cluster.[5] A weaker, broad absorption observed at approximately 370 nm is likely the red-shifted LMCT band. It is unclear why the intensity of this band is so much lower than in the chloride and bromide complexes, but it may be a function of relativistic effects caused by the heavier iodide ligands. As noted above (Figure 2), the position of the dominant Mo 4d final state peak is nearly constant. Therefore, we should consider the possibility that the 285 nm absorption peak of $[Mo_6Cl^i_8Cl^a_4\{P(C_4H_9)_3\}^a]$ also may not be the first MLCT band, as just discussed for the iodine-substituted species. In fact, the calculated peak, corrected for the systematic errors seen in Table 5, of 335 nm would make sense, falling between the Cl^a_6 and Br_6 cases. On the basis of previous experience by many workers, we suppose that substitution of C_4H_9 by H in the calculations has a negligible effect on MLCT transitions.

A second, unbiased approach to the many dipole-allowed transitions can be made via the calculation of the projected joint density of states (PDOS). Here we sum over all dipole-allowed transitions within an interval centered on E_f. The data shown in Figures 7 and 8 represent all transitions from initial states within the first valence band to final states with excitation energy <15 eV. In addition to the prominent low-lying LMCT peak, additional well-defined structures at higher energy are revealed, which invite experimental study. In all the clusters studied, a triple-peak complex appears, spanning an energy of ~5 eV, of which the lowest peak forms the much studied optical band. We have already mentioned some observations of the second, intense band centered at ~4.4 eV in the iodine complex, and possibly, also origin of the "first" peak reported for the phosphine case. Figure 7 shows very clearly the systematic red shift of the halide series, and also reveals weak transitions in the IR which could be of interest. In addition to the one-electron transitions considered here, intraatomic multiplet structures arising within the Mo_6 core should be accessible to IR spectroscopy and may further elucidate the delocalization versus atomic character of the metal atoms. The PDOS (V → M*) results for the first peak, shown in Table 5, confirm the general picture given by HOMO → M* analysis; predicted peak energies are again considerably red shifted with respect to experiment. Because the bipy derivatives have not yet been isolated, no direct comparison with experimental values is possible. PDOS calculations shown in Figure 8 indicate, however, that the main absorption peaks of these compounds will also fall in the near-UV region.

Energy Emission from LUMO to HOMO. Emissive energies are extracted in the simplest approximation as the energy between HOMO and LUMO states, taken in the ground state potential. It is widely accepted that emission occurs via decay of a spin triplet state, associated with the LUMO to HOMO transition.[2-4] We find that transition energies predicted by this method are ~0.6 eV too high (Table 6). Further, uncorrected experimental data show relatively small changes in emissive energies as ligands are altered, with red shifts of 10 nm (0.01 eV) and 30 nm (0.06 eV) for the bromide- and iodide-substituted clusters relative to $[Mo_6Cl^i_8Cl^a_6]^{2-}$, while our calculations predict much larger changes, particularly for the iodide and phosphine substituted clusters. The precision of our experimental emission energy data is limited by the response of the photomultiplier tube at the low wavelengths where these clusters fluoresce. A data correction procedure developed by Newsham *et al.*[23] leads to a pronounced red shift, with changes of 24 nm (0.04 eV) and 57 nm (0.10 eV) for the bromide and iodide substituted clusters relative to the all-chloride cluster. We predict a red shift in emission energies of 19 nm (0.09 eV) and 168 nm (0.60 eV) for the bromide and iodide clusters, using the HOMO/LUMO scheme. These experimental and theoretical results suggest again that the HOMO and LUMO are not dominated by metal character as predicted by simpler theoretical models of the clusters, and are instead heavily mixed with ligand states.

Our results predict a dipole forbidden LUMO to HOMO transition for the chloride, bromide, and iodide clusters, and this is corroborated experimentally by the unusually long-lived emissive states of the Cl, Cl/Br, and Cl/I clusters. The DV results predict a dipole allowed b_1 LUMO to b_1 HOMO transition for the bis(phosphine) compound, and, therefore, a short-lived emissive state. The emissive lifetime of this compound has not been reported. The hypothetical bipy monomer and dimer show many transitions, beginning in the far-IR. Thus, the conjugated bipy ligand appears to compress the HUMO/LUMO gap of the cluster as well as decrease the energy of the first allowed transition (band gap). Because of the large number of allowed transitions at low energies, we also predict rapid deexcitation processes will dominate in these

(22) Bain, R. L. Ph.D. Thesis, Northwestern University, 1995.
(23) Newsham, M. D. *Excited-State Properties of Transition Metal Complexes in Solution and the Solid State*, Thesis, Ph.D. Dissertation, Michigan State University, 1988.

compounds, resulting in short emissive lifetimes. Recently, evidence for electronic conduction in a three-dimensionally bridged extended structure, formed by reaction of $[Mo_6Cl_8i(SO_3CF_3)_6a]^{2-}$ with 4,4′-bipyridine has been discovered.[22] Scanning electron microscopy (SEM) analysis of the extended structure reveals no significant charge buildup on the sample. This is consistent with semiconducting, small band gap behavior and contrasts with observed insulating character of the other Mo_6 compounds studied by SEM and other methods.

Nature of the Excited State. Both general experience and the foregoing comparisons show that a simple HOMO/LUMO transition using ground state (GS) orbitals is unable to give a quantitative account of triplet → singlet emission. We have further examined the nature of the excited state by considering excited state potential relaxation and spin-coupling effects for the $[Mo_6Cl^i_8Cl^a_6]^{2-}$ case. We find the ground state to be $^1A_{1g}$, in agreement with previous theoretical calculations[7] and experimental evidence.[2a] The absorption maximum is presumably determined by dipole-allowed single particle transitions to excited levels. Our model predicts the first allowed transition, approximately 1.5 eV below the absorption maximum, to be $3t_{2u}$ to $6t_{1g}$ at 2.64 eV; however, electronic and geometric relaxation in the excited state can alter this value. Using DF theory, we can accurately estimate the effect of electronic relaxation on excitation energies by performing transition state (TS) calculations.[24] In this scheme, the SCF procedure is modified such that the single-particle excitation energies accurately reflect the many-body excitation spectrum. A TS calculation corresponding to the above excitation yields an energy of 2.42 eV, indicating that the potential for low-lying excited states is not very different from that of the ground state. The relatively small TS difference in comparison to GS predictions is due to the diffuse character of both initial and final states.

Additional information can be gained through calculations involving the triplet state that take into account symmetry and spin-coupling. The $(t_{2u}^5\ e_u^1)$ configuration, resulting from the HOMO to LUMO electron transition, can lead to A_{1g}, T_{1g}, T_{2g}, and E_g triplet states. Thus, possible transitions back to the $^1A_{1g}$ ground state are both spin and orbitally forbidden, as suggested by the long emissive lifetime of the cluster. We compare these results to those of Azumi *et al.*, who suggest that the emissive state arises from a $(t_{2g}^5,\ t_{1u}^1)$ configuration, with $^3T_{1u}$ as the lowest triplet state of the possible T_{2u}, E_u, T_{1u}, and A_{1u} multiplets.[3] Of these sublevels, only the T_{1u} representation can couple with the ground state by an allowed dipole transition.[3] Azumi *et al.* derived these assignments by applying ZDO and other approximations to the matrix elements of a Cotton–Haas "metal-only" model, which neglects any ligand interactions. Spin–orbit splitting of the Mo_6 metal core O_h symmetry levels was included in the model by application of the Boltzmann distribution in modeling temperature dependence of the emission, with use of atomic spin–orbit approximations.

Considering the imprecision of the orbital models applied by Azumi et al., it is not surprising that their assignment of the triplet state differs from ours. However, their approach raises the important issues of spin–spin and spin–orbit coupling effects on optical spectra. We have calculated the DF configuration-average triplet state of the configuration $^3\Gamma(t_{2u}^5\ e_u^1)$ and find that the unpaired spin is delocalized over Mo and axial Cl sites. The significant components are the 4d Mo (0.186), 3p Cl^i (0.026), and 3p Cl^a (0.108) spin/atom. This result reveals that any quantitative model of the triplet excitations must take into account delocalization of the triplet spin over the entire cluster. The triplet to ground state singlet configuration average transition energy can also be calculated by the TS approach. The general formula,

$$\Delta E_{tot} = \sum_i \Delta n_i \epsilon_i^* \qquad (4)$$

where Δn_i is the difference in orbital occupation numbers between initial and final states and ϵ_i^* are the TS orbital eigenvalues, gives the result 2.53 eV. This value is greater than the ground state HOMO/LUMO gap (2.42 eV) and less than the dipole-allowed absorption energy (2.64 eV) cited previously; however, the difference between these values is small. It should be noted that the configuration average is an upper bound of the luminescence energy. We calculated the spin–orbit splittings of the isolated $Mo^{+0.6}$ and $Cl^{-0.3}$ ions in configurations close to the SCF results in order to obtain an estimate of splittings between multiplets. The values for Δ(Mo 4d) = 0.21 eV and Δ(Cl 3p) = 0.06 eV suggest that the magnitude of the spin–orbit splitting is dominated by the Mo 4d contribution. Saito *et al.* report that the luminescence of the $[Mo_6Cl^i_8Cl^a_6]^{2-}$ cluster is red-shifted by approximately 1000 cm^{-1} (0.13 eV) as temperature decreases from 300 to 4.2 K.[11] This indicates that the multiplet levels of the emissive triplet state span an energy range of at least 0.13 eV. Saito also calculates the value of ζ_{Mo} (where $\Delta(Mo) = {}^5/_2\zeta_{Mo}$) to be approximately 610 cm^{-1}, which appears to be consistent with experiment. Our calculations are in fairly good agreement, predicting the value of ζ_{Mo} to be 0.084 eV, or 677 cm^{-1}. If we define the TS configuration average (2.53 eV) to be the center of the emissive energy band, and the band-width to be approximately 1000 cm^{-1}, we estimate the lowest multiplet lies approximately 500 cm^{-1} below the TS average (2.44 eV). This energy difference is approximately equal to ζ_{Mo}, and indicates that spin–orbit splitting contributes relatively little to the discrepancy between experimental and theoretical emission values. The remaining difference in energy may be due to geometric relaxation of the excited state. This would be consistent with ligand-to-metal charge redistribution. The possibility of geometric changes in the excited state is further supported by results of EPR experiments conducted on the $[Mo_6Cl^i_8Cl^a_6]^-$ ion, which suggest the (electrochemically generated) oxidized cluster is axially distorted.[2a] Given that both the $[Mo_6Cl^i_8Cl^a_6]^{2-*}$ excited state and the ground state $[Mo_6Cl^i_8Cl^a_6]^-$ ions are generated by removal of one electron from the HOMO, axial distortion might also be expected to occur in the excited state.

Conclusion

The DV–Xα calculations of the $[Mo_6Cl^i_8L^a_6]^n$ ($n = 0, -1, -2$) system provide information about ligand effects on the electronic structure of the clusters as well as insight into the nature of the excited state. We find that substitution of axial ligands has a subtle influence upon the composition of the discrete HOMO and LUMO states. Perhaps more significant, however, is that the DOS profiles of the unbridged clusters are very similar, regardless of the number or identity of the ligands replacing axial chlorides of the basic $[Mo_6Cl^i_8Cl^a_6]^{2-}$ unit. This means not only that $Mo_6X^i_8$ is a very stable component, but also that the $Mo_6X^i_8L^a_6$ moiety has a well-defined and stable electronic structure, with inner and outer ligand spectroscopic properties fairly well separated in energy. The Mo 4d states are only lightly perturbed by ligand substitution, indicating that the metal–metal bonding of the clusters is hardly influenced

(24) Slater, J. C. *The Self-Consistent Field for Molecules and Solids*; McGraw-Hill: New York, 1974.
(25) Robinson, L. M.; Bain, R. L.; Ellis, D. E.; Shriver, D. F. Manuscript in preparation.

by axial ligands. Significant occupancy of metal 5s and 5p levels provides a conduction electron sea which can be easily displaced by greater or less electron-withdrawing ligands, and provides a means for intercluster charge transport. DOS diagrams and PDOS optical transition predictions provide convincing evidence that the dominant energy absorption of the variously substituted clusters into the first strong absorption band involves predominantly axial ligand to metal charge transfer.

In addition, several pieces of information regarding the nature of the ground state and emissive state can be extracted from the calculations. First, our model predicts that the pure halide clusters have a closed-shell ground state configuration ^1A_g, as confirmed by experimental evidence.[2a] Second, the transition from LUMO to HOMO is predicted to be dipole forbidden for $[Mo_6Cl^i_8Y^a_6]^{2-}$, Y = Cl, Br, and I, as is corroborated by the unusually long-lived emission of the Cl, Br, and I clusters. The bis(phosphine) and bipy clusters have much lower symmetry and thus have fewer orbitally forbidden transitions. As a result, these complexes are predicted to have shorter lived emissive states.

Transition state calculations involving the LUMO to HOMO transition show that *electronic* relaxation plays a relatively small role in modifying the emissive energy (estimated as the energy of the HOMO/LUMO gap) predicted using the ground state levels. This is due to the rather delocalized metal−ligand valence orbital character. Similarly, ground state eigenvalues were used to predict main low-lying absorption features. On the other hand *geometric* relaxation of the molecular framework in the LMCT excited optical state and in the emissive triplet state is quite probable and may be responsible for the systematic shifts found in comparing theoretical and experimental absorption and emission energies. A further possibility, to be explored in future work, is that calculation of oscillator strengths may shift the theoretical band maximum.

Spin-polarized excited state calculations indicate the position of the band-center, or configuration average of the emissive triplet state, to be 2.53 eV. It will be necessary to determine the spin−orbit splitting of the delocalized MO's, which is certainly less than that of the isolated metal (Relativistic LD results predict spin−orbit splitting Δ(Mo 4d) = 0.21eV for the self-consistent ion in the cluster; Saito *et al.* predict 0.15 eV for the neutral atom), in order to resolve the individual multiplet components. Since indirect relativistic level shifts are of the same magnitude, we must defer further discussion to a future article, where a proper relativistic description is made.[24]

Our studies of the hypothetical 4,4′-bipyridine monosubstituted cluster and on the bridged dimer predict that these complexes, when synthesized, will retain many of the recognizable features of the halide- and phosphine-substituted species. In addition, the very wide spectral distribution of bonded N 2p levels, spanning the entire valence and low-lying excitation region, shows that bipy-linked extended structures should strongly couple Mo_6 cores, providing facile pathways for electronic transport. The dimer is predicted to be a small gap semiconductor and this is indirectly supported by SEM data on three-dimensional bridged species; nevertheless, the main LMCT absorption peaks fall at about the same location as in the phosphine compound. Formation of chains and cross-linked arrays would doubtless further reduce the band gap and may result in an interesting class of molecular metals.

Acknowledgment. This work was supported in part by the MRL program of the National Science Foundation, at the Northwestern University Materials Research Center, under Award No. DMR-9120521, the National Science Foundation Award No. CHE-9014662 and a National Science Foundation Graduate Fellowship (L.M.R.). Calculations were carried out in part at the National Center for Supercomputer applications at the University of Illinois at Urbana-Champaign using Cray YMP and Convex C3 systems.

IC940671W